Thermal Radiation in Rayleigh-Bénard Instability

J. H. Lienhard V
Department of Mechanical Engineering,
Massachusetts Institute of Technology,
Cambridge, MA 02139
Mem. ASME

Thermal radiation from finite-conductivity boundaries can strongly affect the stability of horizontally unbounded, plane fluid layers heated from below. The role of thermal radiation in plane layer instabilities is studied under the assumption that the fluid medium is transparent, as a model of infrared transfer through gas layers. The solution procedure modifies a previous formulation of the conductive boundary problem to account for the gray radiant interchange between boundaries. The nonisothermal character of the boundaries is shown to bias instability toward higher wavenumbers and to substantially increase the stability of fluid layers between radiative, nonconductive boundaries relative to layers having nonradiative boundaries. A single layer is studied first, and then a case of parallel, interacting fluid layers is considered. Critical Rayleigh numbers are presented as both tabulations and correlations. The implications for solar collector design are discussed.

1 Introduction

Wall radiation has long been believed to play a significant role in the stability of gas layers heated from below. Theoretical treatments of this problem have been rather limited, however, because radiation can only play an active role when the boundaries are of finite thermal conductivity and the instability with conductive boundary has only been fully treated in recent years. The problem of thermal instability in radiatively participating media has received considerable attention, particularly in the astrophysical literature, but in those cases boundary effects have been generally minimized.

The effects of boundary radiation can be substantial. Edwards and Sun (1971) considered sidewall radiation in thermal instability of diathermanous gases in long vertical cylinders. Their analysis adapted an existing result for conductive sidewalls by introducing an effective conductivity that incorporated the radiant exchange between elements of the sidewalls. They found that wall radiation strongly stabilizes the fluid column.

Various situations of technical interest involve thermal instability in plane air layers at relatively low temperatures. Two prominent examples are the instabilities in air layers within the cover plates of flat-plate solar collectors and the instabilities arising in various building ceiling insulation problems. In such situations, radiant emission from the boundaries is dominantly in the infrared, and the gas layer is essentially diathermanous. In this paper, I consider the effect that thermal radiation may have upon such instabilities.

Previous work on plane layer instabilities (e.g., Lienhard, 1987) has shown that boundaries of low thermal conductivity can support large temperature perturbations (hot and cold spots), which reduce the critical Rayleigh number of a fluid layer by as much as a factor of 2.5. The effect of radiation is to cool hot spots by emission and to warm cold spots by absorption; as a result, radiation stabilizes these otherwise very unstable configurations.

This paper begins with a formulation of the radiant instability for an individual layer, building upon methods introduced in the conductive-boundary stability problem. With this solution, important features of the single-layer instability are explored. Then a coupled fluid layer instability is studied, in a configuration typical of flat-plate solar collectors. The relative importance of thermal radiation in these situations is assessed, and correlations of the numerical results are given.

In a recent work, Richards and Edwards (1989) have treated a similar problem in which boundary temperature disturbances are represented by a heat transfer coefficient. That model effectively requires that the wall have no horizontal thermal diffusivity, as discussed by Lienhard (1987). Some caution is required in applying that approximation, as it can easily lead to errors that are as large as radiative effects. In this work, I consider the opposite limiting case of fully conductive walls. The relation of the two limits is also assessed.

Various other contrasts between these two studies may also be noted. Richards and Edwards allow for spectral wall radiation; the present work has been confined to gray walls. Richards and Edwards consider only rolls at onset of motion and obtain numerical solutions; the present work treats all allowable planforms and presents analytical solutions. The present formulation is valid for an arbitrary number of asymmetric layers with conductive interaction; the other allows for radiative interactions of highly symmetric fluid layers through midlayers having no horizontal diffusivity. This work and that of Richards and Edwards are thus complementary in several respects.

2 Formulation

We have assumed the medium between the plates to be transparent to infrared radiation, and, consequently, the fluid temperature profile in the quiescent state remains linear, as in the nonradiative case. Radiation is apparent only in the calculation of the heat flux at the boundaries of a given fluid layer.

The fluid stability problem thus differs from the classical problem only in the type of boundary conditions to be applied. The fluid itself, in the usual fashion, satisfies a normal mode perturbation solution (Rayleigh, 1916); for steady onset of motion, the general solution for the dimensionless normal mode amplitude of the temperature disturbance in layer i, $\Theta_i(z_i)$, was found by Pellew and Southwell (1940)

$$\Theta_i = A\cosh(qz_i) + A^*\cosh(q^*z_i) + A_0\cos(q_0z_i) + B\sinh(qz_i) + B^*\sinh(q^*z_i) + B_0\sin(q_0z_i) \quad (1)$$

where $(\,)^*$ denotes a complex conjugate, A and B are unknown constants, and

$$q_0 = a_i(\tau-1)^{1/2},\quad q^2 = a_i^2\left(1+\frac{1}{2}\tau(1\pm i\sqrt{3})\right),\quad \text{with } \mathrm{Ra}_i = a_i^4\tau^3 \quad (2)$$

The Rayleigh number of layer i is an eigenvalue of this equation, determined by application of the boundary conditions. An analogous analysis of the heat equation shows that the temperature perturbation in a solid boundary is given by

Contributed by the Heat Transfer Division for publication in the JOURNAL OF HEAT TRANSFER. Manuscript received by the Heat Transfer Division November 18, 1988. Keywords: Natural Convection, Radiation Interactions, Solar Energy.

$$\Theta_B(z_B) = M \cosh(a_B z_B) + N \sinh(a_B z_B) \quad (3)$$

for unknown constants M and N. More specific features of the present development appear in the usual literature.

Scaling. The nondimensionalization is based on the scales of an individual layer. In fluid layer i, temperature is scaled with its difference across the layer, ΔT_i, and length is scaled with the layer thickness, L_i. In a solid wall of finite thickness, temperature is scaled with its difference across the wall, ΔT_B, and length is scaled with the wall thickness, L_B. In a semi-infinite wall, temperature and length are scaled with the scales of the adjacent fluid layer. Wavenumbers are nondimensionalized with the length scale of the layer in which they are considered. For example, $a_i = 2\pi L_i/\lambda$ and $a_B = 2\pi L_B/\lambda$. The disturbance wavelength λ clearly has the same value in every layer.

2.1 Boundary Conditions. The fluid layer is contained between rigid walls at $z = \pm 1/2$ for which the no-slip condition applies. From this condition, one obtains (Lienhard, 1987) the following relations among the coefficients of the solution:

$$\begin{bmatrix} \cosh(q/2) & \cosh(q^*/2) \\ q\sinh(q/2) & q^*\sinh(q^*/2) \end{bmatrix} \begin{bmatrix} (q^2-a^2)A \\ (q^{*2}-a^2)A^* \end{bmatrix} = A_0(q_0^2+a^2)\begin{bmatrix} \cos(q_0/2) \\ -q_0\sin(q_0/2) \end{bmatrix} \quad (4)$$

and

$$\begin{bmatrix} \sinh(q/2) & \sinh(q^*/2) \\ q\cosh(q/2) & q^*\cosh(q^*/2) \end{bmatrix} \begin{bmatrix} (q^2-a^2)B \\ (q^{*2}-a^2)B^* \end{bmatrix} = B_0(q_0^2+a^2)\begin{bmatrix} \sin(q_0/2) \\ q_0\cos(q_0/2) \end{bmatrix} \quad (5)$$

These conditions determine A and B in terms of A_0 and B_0.

Thermal boundary conditions are the matching of fluid and solid temperature and heat flux. These conditions reduce to a matching of perturbation temperature and flux, which fixes A_0 and B_0. The difficulty encountered in the radiative problem is the calculation of the radiant perturbation.

2.2 Radiant Exchange. The perturbation to the basic temperature field renders the boundaries nonisothermal, and this perturbation radiant exchange enters the boundary condition for the stability problem. Hence, the calculation of the radiant exchange must account for the variation in surface temperature; integration is required.

Prior to calculating the radiant exchange between two gray walls, it is convenient to find the radiation incident on an element of one wall that is emitted by an opposing black wall when the temperature field experiences a small wavelike perturbation of planform $f(x,y)$. The perturbed temperature along the opposing wall (wall 2, say) is

$$T_2(x,y) = \bar{T}_2 + \tilde{T}_2 f(x,y) \quad (6)$$

for mean temperature $\bar{T}_2$ and perturbation $\tilde{T}_2$, and the linearized radiant emission at any point is thus

$$\sigma T_2^4 = \sigma(\bar{T}_2^4 + 4\bar{T}_2^3\tilde{T}_2 f(x,y)) = \sigma\bar{T}_2^4 + \Delta_2 f(x,y) \quad (7)$$

where $\Delta_2 = 4\sigma\bar{T}_2^3\tilde{T}_2$ is the amplitude of the normal mode radiative emission at wall 2.

The radiation received at an element of wall 1 may be found by integrating the differential flux received from an element of wall 2 over surface 2. The differential flux is

$$d^2q_1^- = \sigma T_2^4(r,\theta)\, dF_{d2-d1}\frac{dA_2}{dA_1} = \sigma T_2^4(r,\theta)\frac{1}{\pi(r^2+1)^2} r\,dr\,d\theta \quad (8)$$

We have introduced a polar coordinate system on surface 2 with origin above the differential element of surface 1 to facilitate the integration (see Fig. 1). Lengths have been scaled with the plate spacing L_i, leaving other variables in dimen-

Nomenclature

a_i = dimensionless wavenumber in layer $i = 2\pi L_i/\lambda$
A = midlayer to fluid layer aspect ratio $= L_B/2L_i$
A, A_0, B, B_0 = unknown coefficients of the temperature normal mode amplitude, equations, (1), (4), (5) and Appendix A
dF_{d1-d2} = view factor between a differential element of surface 1 and a differential element of surface 2
D_i = dimensionless vertical derivative in layer $i = d/dz_i$
$f(x,y)$ = dimensionless solution of the Helmholtz equation
g = gravitational body force
k, k_B = thermal conductivity of the fluid or boundary
$K_1(a)$ = modified Bessel function of first order
L_i, L_B = thickness of fluid layer i or midlayer B
N_i = radiation/conduction parameter at wall $i = 4\sigma T_i^3 L_i/k$
q, q_0, τ = see equations (1) and (2)
q_{12} = net base state radiant heat flux $= \sigma(T_1^4 - T_2^4)/(1/\epsilon_1 + 1/\epsilon_2 - 1)$
q_{bs} = net base state heat flux
q_i^- = incoming radiant heat flux at wall i
$\tilde{q}_i^+, \tilde{q}_i^-$ = outgoing/incoming radiant perturbation heat flux at black wall i
$\tilde{q}_i$ = net perturbation radiant flux leaving wall i
(r, θ) = dimensionless polar coordinates in the horizontal plane
Ra_i, Ra_c = critical Rayleigh number for layer $i = g\beta L_i^3\Delta T_i/\nu\alpha$
$T(x,y,z), \tilde{T}(x,y,z)$ = dimensional fluid temperature distribution, fluid temperature perturbation
$T_i, \bar{T}, \tilde{T}_i$ = dimensional temperature, mean (base state) temperature, and perturbation temperature of wall i

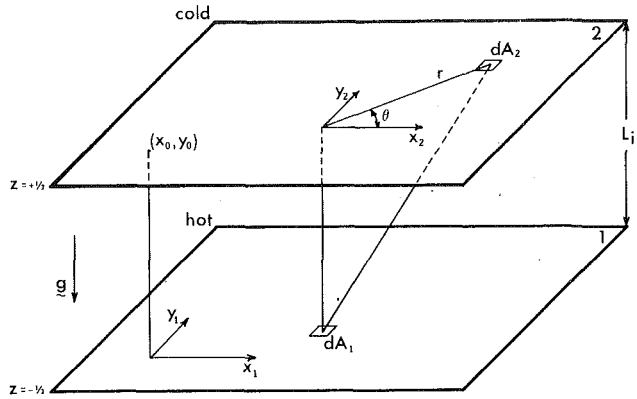

Fig. 1 Geometry and coordinate systems

sional form. This allows us to use the dimensionless planform and wavenumber of the stability analysis without becoming ensnared in additional nomenclature. The incoming flux at surface 1 is then $q_1^- = \sigma \bar{T}_2^4 + \tilde{q}_1^-$, where the radiant perturbation is given by the integral

$$\tilde{q}_1^- = \frac{\Delta_2}{\pi} \int_0^\infty \int_0^{2\pi} \frac{f(r,\theta) r dr d\theta}{(r^2+1)^2} \tag{9}$$

in which r, f, and the wavenumbers are dimensionless.

2.3 Planform at Onset. To integrate the radiative exchange over the boundaries, some assumption as to the planform at onset of motion must be introduced. The normal mode analysis shows that the planform at onset, $f(x,y)$, must satisfy the Helmholtz equation $(\partial^2 f/\partial x^2 + \partial^2 f/\partial y^2 + a^2 f = 0)$; no more specific assumptions are needed.

Experimentally the planform is most often observed to be either rolls or hexagons near onset of motion, although the presence of vertical sidewalls in most laboratory situations will influence the specific mode observed. Here we compute the radiant perturbations for a general planform, which includes those planforms as special cases. Somewhat surprisingly, the results are identical for *all* planforms. We thus show that radiant stabilization does not favor one mode of onset over any other.

Several coordinate systems are required in evaluation of the integrals (see Fig. 1): (x_1, y_1) and (x_2, y_2) are Cartesian systems on A_1 and A_2, respectively; the integrals over A_2 are most conveniently phrased in polar coordinates, (r, θ), which coincide with (x_2, y_2). The origin of the (x_1, y_1) system may be placed at the origin of planform symmetry for convenience, and the origin of the (x_2, y_2) system may be located above the point (x_1, y_1) at which the incident radiation is to be calculated. The origin of symmetry (x_0, y_0) is located in the A_2 coordinates, and it follows that (x_0, y_0) has the value $-(x_1, y_1)$.

Bisshopp (1960) has found the most general planform that has x and y periodicities characterized by a given total wavenumber a (cf. Chandrasekhar, 1961):

$$f(x, y) = C \cos\left[a\left(1 - \frac{1}{m^2}\right)^{1/2} x\right] \cos \frac{a}{m} y + \cos ay \tag{10}$$

for m an integer greater than 1, C a constant, and a the total wavenumber.[1] This equation may be recast into polar coordinates, letting $\kappa = (1 - 1/m^2)^{1/2}$

$$\begin{aligned} f(r,\theta) = \frac{C}{2}\Bigg\{ & \cos\left[ar\left(\frac{\cos\theta}{\kappa} + \frac{\sin\theta}{m}\right)\right] c_-(x_0, y_0) \\ & + \sin\left[ar\left(\frac{\cos\theta}{\kappa} - \frac{\sin\theta}{m}\right)\right] s_-(x_0, y_0) \\ & + \cos\left[ar\left(\frac{\cos\theta}{\kappa} + \frac{\sin\theta}{m}\right)\right] c_+(x_0, y_0) \\ & - \sin\left[ar\left(\frac{\cos\theta}{\kappa} + \frac{\sin\theta}{m}\right)\right] s_+(x_0, y_0) \\ & + \cos(ar\sin\theta)\cos ay_0 + \sin(ar\sin\theta)\sin ay_0 \Bigg\} \end{aligned} \tag{11}$$

[1] For rolls, $m = 1$; for hexagons, $C = 2$, $m = 2$.

Nomenclature (cont.)

$W(z)$ = dimensionless normal mode amplitude of vertical fluid velocity
(x, y, z) = dimensionless Cartesian coordinates, z vertical and increasing upward
X_i = ratio of fluid thermal conductivity to wall i conductivity
X_B = fluid to midlayer (or boundary) thermal conductivity ratio
α = midlayer temperature disturbance coupling parameter or fluid thermal diffusivity, by context
Δ_i = dimensional amplitude of normal mode radiant emission at wall $i = 4\sigma \bar{T}_i^3 \tilde{T}_i$
ΔT_i = temperature difference across layer i
ϵ_i = gray body emissivity of wall i
$\Theta_i(z)$ = dimensionless normal mode temperature disturbance amplitude in layer i
λ = dimensional disturbance wavelength
Λ_{ij} = coefficient of third-kind boundary condition, defined where used
ν = kinematic viscosity
σ = Stefan-Boltzmann constant
ψ = $aK_1(a)$
Ψ_a, Ψ_b = reflection functions defined by equations (23) and (24)
$\Im$ = imaginary part of a complex number
$\Re$ = real part of a complex number

Superscripts and Subscripts

$(\ )^*$ = complex conjugate
$(\tilde{\ })$ = a perturbation
$(\ )_B$ = quantity referred to the midlayer or boundary, or quantity nondimensionalized in midlayer or boundary scales
$(\ )_i$ = quantity referred to fluid layer i or nondimensionalized in scales of fluid layer i

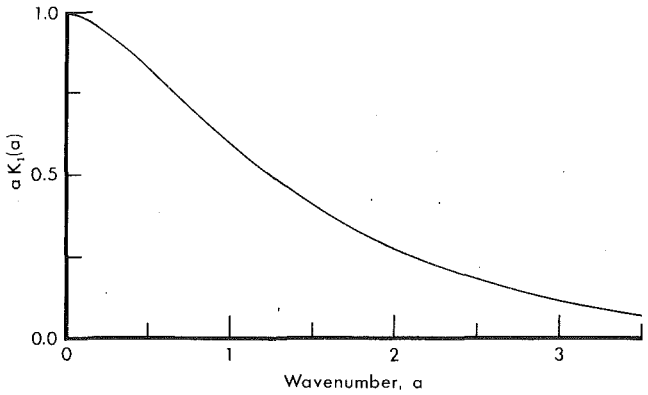

Fig. 2 Attenuation factor

where we use the notation $c_{\pm}(x_0, y_0) = \cos a(x_0/\kappa \pm y_0/m)$ and $s\pm(x_0, y_0) = \sin a(x_0/\kappa \pm y_0/m)$. With some calculation, the integral for this planform may be reduced to

$$\tilde{q}_1^-(x_1, y_1) = \frac{\Delta_2}{\pi}\left[\cos ay_0 + \frac{C}{2}(c_- + c_+)\right] \times \int_0^\infty \frac{r}{(r^2+1)^2}\int_0^{2\pi} \cos(ar \sin\theta)\, d\theta\, dr$$

$$= 2\Delta_2\left[\cos ay_0 + \frac{C}{2}(c_- + c_+)\right]\int_0^\infty \frac{rJ_0(ar)\,dr}{(r^2+1)^2} \tag{12}$$

in which we have identified the integral representation of the first kind Bessel function of order zero, J_0

$$J_0(z) = \frac{1}{\pi}\int_0^\pi \cos(z \sin\theta)\, d\theta \tag{13}$$

The remaining integral may be evaluated, so producing

$$\tilde{q}_1^-(x_1, y_1) = aK_1(a)\Delta_2 f(x_0, y_0) = aK_1(a)\Delta_2 f(x_1, y_1) \tag{14}$$

where K_1 is a modified Bessel function of first order. The result is the opposing wall perturbation radiosity multiplied by an attenuation factor dependent upon the wavenumber. Richards and Edwards (1989) also obtained this factor for a roll planform, although their result is in numerical form. (Their $S(a)$ is actually $aK_1(a)$.)

Evidently, the form of the attenuation factor is a property of the present averaging of unbounded, symmetric solutions of the Helmholtz equation.

The physical interpretation of these results relates simply to the periodic variations in radiant emission from the surface being viewed. The attenuation factor (Fig. 2) represents the reduction in net radiation incident from the surface viewed caused by increasing the spatial frequency of surface temperature variations. When the surface temperature varies rapidly (large a), the point considered receives little net perturbation transmission: The perturbation flux averages out. When the spatial variation is slow (small a), little averaging occurs because the surface as viewed is largely isothermal. Similarly, the flux received at any point depends on its location relative to the hot and cold peaks of the wavelike perturbation. At a hot peak of the wave, the radiation perturbation is greatest; at a node of the wave, the radiation perturbation is zero.

The radiative transport shows a significant dependence upon the wavenumber. Edwards and Sun (1971) were able to incorporate radiative effects into an effective wall conductivity in their study of sidewall radiation in circular cylinders, by deducing a priori the most unstable wavenumber in their horizontally bounded domain. The horizontal domain of the present problem is unbounded, and the wavenumber may vary continuously. As a result, radiation effects will influence the critical wavenumber, and the wavenumber at onset of motion cannot generally be inferred from other considerations.

2.4 Net Radiant Exchange. The boundary conditions of the stability analysis require us to know the net radiant exchange along both surfaces. For two black walls, the perturbation exchange follows directly from the preceding results:

$$\tilde{q}_1(x, y) = \tilde{q}_1^+(x, y) - \tilde{q}_1^-(x, y) = (\Delta_1 - aK_1(a)\Delta_2) f(x, y) \tag{15}$$

For gray walls, the exchange problem is complicated by reflection between the two walls. Richards and Edwards (1989) solved this problem using a radiosity-irradiation approach. Here we sketch an alternate (although longer) solution using a net-radiation method.

The radiant interchange can be expressed in terms of a pair of coupled integral equations relating the wall temperature distributions to the net heat flux *leaving* each point on the two surfaces (Siegel and Howell, 1981, §8-4.1). Upon deducting the base state radiant exchange q_{12} from those equations we obtain a similar pair of coupled equations describing the perturbation exchange

$$\frac{\tilde{q}_1(x_1, y_1)}{\epsilon_1} - (1-\epsilon_2)\int_{A_2}\frac{\tilde{q}_2(x_2, y_2)}{\epsilon_2} dF_{d1-d2} = (\Delta_1 - aK_1(a)\Delta_2) f(x_1, y_1) \tag{16}$$

$$\frac{\tilde{q}_2(x_2, y_2)}{\epsilon_2} - (1-\epsilon_1)\int_{A_1}\frac{\tilde{q}_2(x_2, y_2)}{\epsilon_2} dF_{d2-d1} = (\Delta_2 - aK_1(a)\Delta_1) f(x_2, y_2) \tag{17}$$

These equations decouple if one wall (wall 1, say) is black. In that case, $\tilde{q}_2$ is obtained directly and $\tilde{q}_1$ by a second integration

$$\tilde{q}_1(x, y) = \{\Delta_1[1-(1-\epsilon_2)(aK_1(a))^2] - \epsilon_2 aK_1(a)\Delta_2\} f(x,y) \tag{18}$$

$$\tilde{q}_2(x, y) = \epsilon_2\{\Delta_2 - aK_1(a)\Delta_1\} f(x,y) \tag{19}$$

The attenuation factor appears squared as a result of the reflection integration of $\tilde{q}_1$.

The appearance of powers of $aK_1(a)$ in the gray-black solution, deriving from the partial reflection at the gray wall, suggests that the gray-gray solution, involving an infinite sequence of such partial reflections[2], will be expressible as a power series in $aK_1(a)$. Thus, we attempt the general solution of equations (16) and (17) using the forms

$$\frac{\tilde{q}_1}{\epsilon_1} = \left(\sum_{n=1}^\infty A_n\psi^n\right) f(x, y) \text{ and } \frac{\tilde{q}_2}{\epsilon_2} = \left(\sum_{n=1}^\infty B_n\psi^n\right) f(x, y) \tag{20}$$

with $\psi = aK_1(a)$. Substituting these into equations (16) and (17) and equating coefficients of like powers of ψ, we obtain four geometric series in $(1-\epsilon_1)(1-\epsilon_2)\psi^2$, which may each be summed, producing a closed-form solution. The dimensional normal mode radiant perturbation flux leaving each wall is thus found to be

$$\tilde{q}_1 = 4\sigma\Delta T_i\{\bar{T}_1^3\Psi_a(\epsilon_1, \epsilon_2, a)\Theta_i(-1/2) - \bar{T}_2^3\Psi_b(\epsilon_1, \epsilon_2, a)\Theta_i(1/2)\} f(x, y) \tag{21}$$

[2] Recall the ray tracing derivation of the view factor for infinite parallel plates.

$$\tilde{q}_2 = 4\sigma \Delta T_i \{ -\bar{T}_1^3 \Psi_b(\epsilon_2, \epsilon_1, a)\Theta_i(-1/2) + \bar{T}_2^3 \Psi_a(\epsilon_2, \epsilon_1, a)\Theta_i(1/2)\} f(x, y) \quad (22)$$

where we have defined the following transfer factors

$$\Psi_a(\epsilon_1, \epsilon_2, a) = \epsilon_1 \left(1 - \frac{\epsilon_1(1-\epsilon_2)\psi^2}{1-(1-\epsilon_1)(1-\epsilon_2)\psi^2}\right) \quad (23)$$

$$\Psi_b(\epsilon_1, \epsilon_2, a) = \epsilon_1 \epsilon_2 \left(\frac{\psi}{1-(1-\epsilon_1)(1-\epsilon_2)\psi^2}\right) \quad (24)$$

These functions account for the absorption and reflection of radiation; the order of the arguments, ϵ_i, of Ψ_a must be reversed at the opposing wall. These are identical (for gray walls) to the transfer factors F_0 and F_{01}, respectively, obtained by Richards and Edwards.

2.5 Thermal Boundary Conditions. Having the general radiative boundary condition, we are now able to form the thermal boundary conditions on the normal mode amplitudes. The matching of temperatures, under the present scaling, yields

$$\Theta_i = \left(\frac{k_i}{k_B}\right)\left(\frac{L_B}{L_i}\right)\Theta_B \quad (25)$$

for walls of finite thickness, and

$$\Theta_i = \Theta_B \quad (26)$$

for semi-infinite walls. The matching of the perturbation heat flux must incorporate the radiative transfer. In physical variables, for Z the dimensional vertical coordinate,

$$-k_i \left.\frac{d\tilde{T}}{dZ}\right|_1 + \tilde{q}_1 = -k_B \left.\frac{d\tilde{T}_B}{dZ}\right|_1 \quad (27)$$

at wall one and

$$-k_i \left.\frac{d\tilde{T}}{dZ}\right|_2 = -k_B \left.\frac{d\tilde{T}_B}{dZ}\right|_2 + \tilde{q}_2 \quad (28)$$

at wall two. In nondimensional form, the conditions on the normal mode amplitudes at walls of finite thickness become

$$D_i\Theta_i(-1/2) = \left(\frac{k_B}{k_i}\right)\left(\frac{L_i}{L_B}\right)\left(\frac{\Delta T_B}{\Delta T_i}\right) D_B\Theta_{B_1}(1/2) + \left(\frac{L_i}{k_i \Delta T_i}\right)\frac{\tilde{q}_1}{f(x, y)} \quad (29)$$

$$D_i\Theta_i(1/2) = \left(\frac{k_B}{k_i}\right)\left(\frac{L_i}{L_B}\right)\left(\frac{\Delta T_B}{\Delta T_i}\right) D_B\Theta_{B_2}(-1/2) - \left(\frac{L_i}{k_i \Delta T_i}\right)\frac{\tilde{q}_2}{f(x, y)} \quad (30)$$

where the fluid and solid layer normal mode amplitudes are scaled with variables appropriate to the individual layers. For semi-infinite walls, the normal mode amplitudes are scaled with the fluid layer thickness and temperature difference

$$D_i\Theta_i(-1/2) = \left(\frac{k_B}{k_i}\right) D_B\Theta_{B_1}(0) + \left(\frac{L_i}{k_i \Delta T_i}\right)\frac{\tilde{q}_1}{f(x, y)} \quad (31)$$

$$D_i\Theta_i(1/2) = \left(\frac{k_B}{k_i}\right) D_B\Theta_{B_2}(0) - \left(\frac{L_i}{k_i \Delta T_i}\right)\frac{\tilde{q}_2}{f(x, y)} \quad (32)$$

Using methods developed in an earlier work (Lienhard, 1987), the wall temperature disturbances may be eliminated from these boundary conditions to produce a third kind condition to be applied directly to the fluid temperature disturbance at either boundary of the fluid layer. The procedure consists of using the exact solution for $\Theta_B(z)$ to eliminate $D\Theta_{B_j}$ in favor of Θ_{B_j}, which is then replaced with $\Theta_i(\mp 1/2)$. (For example, at an upper semi-infinite boundary, $D\Theta_B(0) = -a_B/(k_i/k_B)\Theta_B(0) = -a_i/(k_i/k_B)\Theta(1/2)$.) The resulting conditions have the form

$$D\Theta_i(-1/2) = \Lambda_{11}\Theta_i(-1/2) + \Lambda_{12}\Theta_i(1/2) \quad (33)$$

$$D\Theta_i(1/2) = \Lambda_{21}\Theta_i(-1/2) + \Lambda_{22}\Theta_i(1/2) \quad (34)$$

The Λ_{ij} depend on various physical parameters. Specific examples appear below.

These boundary conditions differ from the usual third kind conditions in that the temperature gradient at either wall depends upon the temperature disturbance at *both* walls. Nonetheless, these boundary conditions may be applied to close the solution with a condition on the remaining unknown coefficients of equation (1), A_0 and B_0:

$$\begin{bmatrix} \mathcal{C}_1 & \mathcal{C}_2 \\ \mathcal{C}_3 & \mathcal{C}_4 \end{bmatrix}\begin{bmatrix} A_0 \\ B_0 \end{bmatrix} = 0 \quad (35)$$

The functions $\mathcal{C}_i$ are given in Appendix A. By determining values of Ra for which the matrix $\mathcal{C}$ is nonsingular, we find the eigenvalues of the stability problem. The smallest eigenvalue is then minimized as a function of wavenumber to give the critical Rayleigh number of the configuration, Ra_c.

2.6 Models of Wall Thermal Behavior. We have taken the wall temperature to satisfy a heat conduction condition. Richards and Edwards treated instead the situation when the wall heat loss is characterized by a convective boundary condition. The difference between the two conditions has been discussed by Lienhard (1987), who found that critical Rayleigh numbers for the conditions differ significantly (differences can be as large as those produced by radiation). In particular, suppose fluid layer i to be bounded by a conductive slab (thickness L_B, conductivity k_B) whose outer side is cooled according to a convection coefficient h_i. Lienhard showed that only when

$$a_i^2\left(\frac{L_B}{L_i}\right)^2 << hL_i/k_i << 1 \quad (36)$$

may the thermal diffusivity of the slab be ignored and the fluid boundary condition represented by a Biot number, hL_i/k_i. Conversely, a slab of arbitrary thermal conductivity will behave as a semi-infinite boundary when

$$\left(a_i \frac{L_B}{L_i}\right) \geq 1.8 \quad (37)$$

In between these two limits, the boundary condition applied must account for *both* the conductive and the convective effects. In this paper, we consider the purely conductive boundary condition.

In all three circumstances, the third-kind boundary condition is wavenumber dependent. Richards and Edwards surmounted this complication with a graphic solution to be used iteratively. Here, we employ the methods developed in the previous work (1987) to facilitate direct solutions for such wavenumber-dependent conditions. Our results are both tabulated and presented as a correlation.

Direct comparison of the present work to the Richard and Edwards results is not possible because the boundary conditions are different. We avoid the tempting, but erroneous, model of a conducting boundary slab (thickness L_B, conductivity k_B) as a heat transfer coefficient $h = k_B/L_B$; this approximation neglects the *horizontal* diffusion of heat in the slab, which damps wall temperature perturbations. A conducting wall solution must account for such transverse heat conduction, as do the boundary conditions used here.

We also note that the differing wavenumber dependences of the conductive and convective boundary conditions will lead

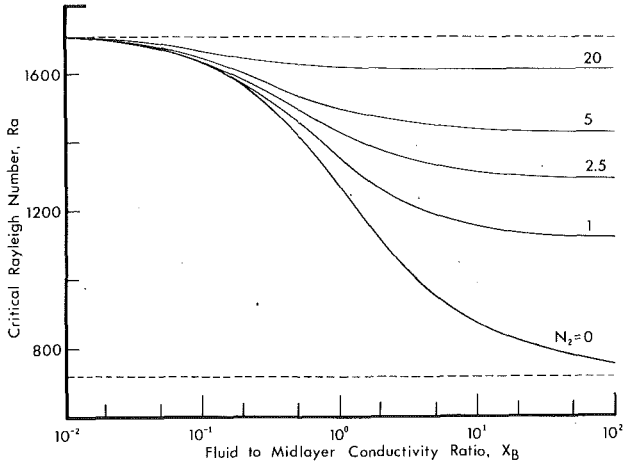

Fig. 3 Single layer with identical, conducting, black walls: $N_1/N_2 = 2$

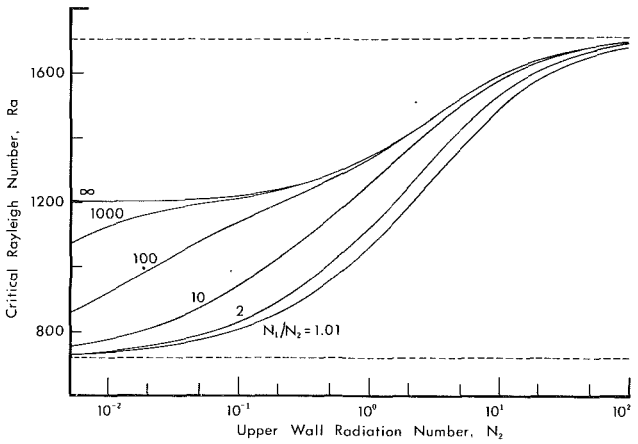

Fig. 4 Fixed heat flux limit of the single layer

Table 1 Critical Rayleigh numbers and wavenumbers for a single layer with identical, semi-infinite, conductive, black walls: $N_1/N_2 = 2$

Critical Rayleigh Number

	Fluid Layer to Wall Conductivity Ratio, X_B							
N_2	0	0.1	0.3	1.0	3.0	10.0	100.0	∞
0.0	1707.76	1628.01	1505.29	1267.47	1037.89	872.10	753.34	720.00
0.5	1707.76	1629.57	1515.34	1315.25	1150.45	1054.16	1007.02	1001.33
1.0	1707.76	1631.06	1524.27	1351.74	1222.96	1153.41	1121.09	1117.27
2.5	1707.76	1635.16	1546.14	1425.76	1350.46	1313.95	1297.86	1296.00
5.0	1707.76	1640.99	1572.11	1495.38	1454.51	1436.26	1428.51	1427.62
20.0	1707.76	1662.09	1636.92	1619.67	1613.02	1610.44	1609.41	1609.29

Critical Wavenumber

	Fluid Layer to Wall Conductivity Ratio, X_B							
N_2	0	0.1	0.3	1.0	3.0	10.0	100.0	∞
0.0	3.116	3.004	2.818	2.398	1.873	1.330	0.641	0.00
0.5	3.116	3.007	2.839	2.514	2.208	2.001	1.888	1.873
1.0	3.116	3.010	2.856	2.594	2.384	2.264	2.205	2.198
2.5	3.116	3.017	2.890	2.737	2.640	2.594	2.574	2.572
5.0	3.116	3.027	2.941	2.853	2.810	2.793	2.785	2.784
20.0	3.116	3.061	3.036	3.023	3.018	3.016	3.016	3.016

to different critical wavenumbers: The constrained variation of the Rayleigh number in the wavenumber/"Biot number" (or Λ_{ij}) space differs for the two problems, and consequently so must the critical loci. No change of variables will cause the problems to become formally identical (see Fig. 2 of Lienhard, 1987).

3 Single Layer With Conductive, Radiating Boundaries

The solution that best illustrates the radiant instability is that for a single layer with semi-infinite walls of finite thermal conductivity. Critical Rayleigh numbers have been calculated for the full range of wall conductivities and temperatures, assuming black walls of equal conductivity.

For semi-infinite boundaries of unequal conductivity and emissivity, equations (31) and (32) yield the following general boundary conditions after elimination of the wall temperature disturbances:

$$D\Theta(-1/2) = \left\{\frac{a}{X_1} + N_1 \Psi_a(\epsilon_1, \epsilon_2, a)\right\}\Theta(-1/2) - N_2 \Psi_b(\epsilon_1, \epsilon_2, a)\Theta(1/2) \quad (38)$$

$$D\Theta(1/2) = N_1 \Psi_b(\epsilon_2, \epsilon_1, a)\Theta(-1/2) - \left\{\frac{a}{X_2} + N_2 \Psi_a(\epsilon_2, \epsilon_1, a)\right\}\Theta(1/2) \quad (39)$$

Here, we have introduced the nondimensional conduction/radiation groups

$$N_1 = \frac{4\sigma \bar{T}_1^3 L}{k} \text{ and } N_2 = \frac{4\sigma \bar{T}_2^3 L}{k} \quad (40)$$

(with $N_1 > N_2$ for unstable stratification) and we have defined $X_i = k/k_i$ for k the thermal conductivity of the fluid and k_i the thermal conductivity of wall i. The terms on the right-hand sides of the boundary conditions represent the heat conducted into the walls (a/X terms) and the radiant transfer at the walls.

For brevity, we consider only the case of identical black walls of conductivity ratio $X_i = X_B$, for which the boundary conditions simplify considerably

$$D\Theta(-1/2) = \left\{\frac{a}{X_B} + N_1\right\}\Theta(-1/2) - N_2 a K_1(a)\Theta(1/2) \quad (41)$$

$$D\Theta(1/2) = N_1 a K_1(a)\Theta(-1/2) - \left\{\frac{a}{X_B} + N_2\right\}\Theta(1/2) \quad (42)$$

Typical results[3] are shown in Fig. 3. The lowest curve is the nonradiative case. As the level of radiation rises, the layer is increasingly stabilized. This stabilizing effect is greater for the less conductive walls (larger X_B). The mechanism of this stabilization is quite clear: Radiation allows hot and cold spots to be cooled or warmed, thus relieving the otherwise large and destabilizing nonuniformities of the nonconductive walls. The isothermal wall condition ($Ra_c = 1707.762$) is approached as the level of radiation becomes very large.

Radiation markedly increases the critical wavenumber in the nonconductive cases that are strongly stabilized (Table 1). This trend represents an interesting competition between the decreasing stability of less conductive boundaries and the increasingly large radiative stabilization at the small critical wavenumbers normally associated with poorly conducting boundaries.

The limiting case of boundaries of vanishing conductivity ($X_B \to \infty$) also corresponds to boundaries of fixed heat flux (since $D\Theta_B \to 0$). All radiation received at a wall is reradiated; however, the combined emission and absorption still act to reapportion heat among the hot and cold regions of the boundary. Thus, radiation maintains its stabilizing influence (Fig. 4). The usual limits ($Ra_c = 720$, 1707.762) appear at low and high levels of radiation; however, when N_1 remains very large while N_2 vanishes, a new limit is reached in which $Ra_c = 1202.17$. For that case, radiant effects are present at both walls, but the primary behavior is that of an additional mode of cooling the lower surface.

Rather than presenting a large compendium of Rayleigh numbers, we give only a limited tabulation and cover the broader range by correlating the numerical data. The form of

[3] Numerical values are accurate to the number of digits shown; errors are less than 5 ppm.

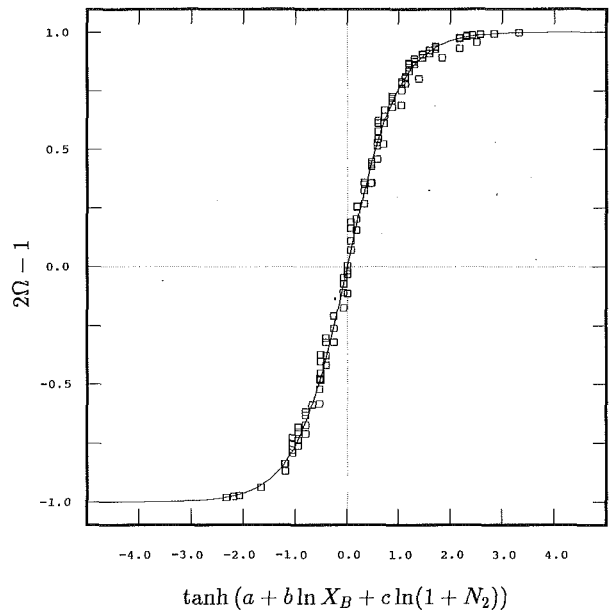

Fig. 5 Correlation of numerical critical Rayleigh numbers for a single layer with semi-infinite, black, conductive walls

the correlation is motivated by the shape of the curves in Fig. 3 and the form of the actual boundary conditions. The Rayleigh number is scaled against its maximum (1707.762) and minimum value (the latter depending on the level of radiation) and is correlated as

$$\Omega = \frac{1707.762 - \mathrm{Ra}_c}{1707.762 - \mathrm{Ra}_{\min}}$$

$$= \frac{1}{2} + \frac{1}{2} \tanh\,[a + b \ln X_B + c \ln(1 + N_2)] \tag{43}$$

The exact solutions for Ra suggest that variations of N_1/N_2 are important in determining $\mathrm{Ra}_{\min}$ but do not affect the shape of the stability boundary. Thus, that parameter is not introduced explicitly in the correlating equation. With exact values of Ra_c spanning the ranges

$$0 \le X_B \le \infty,\ 0 \le N_2 \le 20.0(\to \infty),$$

$$\text{and } 1.0 \le N_1/N_2 \le 10.0 \tag{44}$$

the constants (a, b, c) were determined by least squares to be (-0.077472, 0.48969, 0.37331) to an rms error *in the Rayleigh number* of 1.1 percent and a maximum error of 5.1 percent (see Fig. 5). The ranges of X_B and N_2 cover essentially the complete variation of those parameters; the ratio N_1/N_2 was held below 10 because this covers the range of greatest interest.

In the nonconductive wall case ($X_B \to \infty$), similar considerations lead us to fit Ra_c (which is now $\mathrm{Ra}_{\min}$ in equation (43)) to the form

$$\Omega_\infty = \frac{1707.762 - \mathrm{Ra}_{\min}}{1707.762 - 720.0}$$

$$= \frac{1}{2} + \frac{1}{2} \tanh\,[e + f \ln N_2 + g \ln N_1] \tag{45}$$

Least-squares fitting of (e, f, g) over the ranges

$$0 \le N_2 \le \infty \text{ and } 1.0 \le N_1/N_2 \le 10.0 \tag{46}$$

gives (0.27145, -0.17811, -0.20976) with an rms error *in the Rayleigh number* of 1.8 percent and a maximum error of 4.8 percent. The form of the fit is inadequate to represent the two-step behavior of the stability boundary, which appears at larger values of N_1/N_2. Using equations (43) and (45) for given values of X_B, N_1, and N_2, one may compute Ra_c.

These results may be applied to gas layers with thick boundaries at moderate temperatures. For common materials, the conductivity ratio X_B will always be small when a gas layer is bounded by a solid wall ($X_B < 0.5$). In this range, radiation effects are relatively unimportant, and for such thick boundaries they may almost always be ignored. However, when the boundaries are thin, the effects of finite thermal conductivity are more pronounced because larger temperature gradients can be supported. Thus, radiative effects are quite important for thin layers such as those used as stabilizing partitions in solar collectors. We consider such multilayer problems in the following section. Additional calculations (which are not presented) indicate that reducing the wall emissivity simply decreases the single-layer stability toward the nonradiative limit.

4 Two Layers Separated by a Thin Midlayer

The air gap between a flat-plate solar collector and its coverglass is often partitioned with a thin plastic film in order to reduce natural convection heat loss from the absorber plate. The stability limit of the two layers so formed is coupled by conduction through the separating midlayer (Fig. 6). This behavior has been discussed previously in the absence of thermal radiation (Catton and Lienhard, 1984; Lienhard, 1987). When thermal radiation enters the problem, the base state temperatures are altered and radiation stabilization can also occur.

In this section, we obtain stability results for such a horizontal two-layer configuration. These results are not directly applicable to the finite amplitude convection state, but may be extended to it through such procedures as the power integral method (Lienhard and Catton, 1986). These results should also characterize the finite amplitude heat transfer to the extent that a more stable geometry transfers less heat at a fixed supercritical Rayleigh number. Inclined enclosures of relatively high aspect ratio can be approximated from the horizontal results by using an appropriate effective gravity in calculating the critical Rayleigh number (Hart, 1971).

The wall temperatures satisfy the following equations, which may be solved iteratively for the unknown $\bar{T}_2$ and $\bar{T}_3$:

$$q_{bs} = \frac{k}{L}(\bar{T}_1 - \bar{T}_2) + \frac{\sigma(\bar{T}_1^4 - \bar{T}_2^4)}{1/\epsilon_1 + 1/\epsilon_2 - 1}$$

$$= \frac{k_B}{L_B}(\bar{T}_2 - \bar{T}_3)$$

$$= \frac{k}{L}(\bar{T}_3 - \bar{T}_4) + \frac{\sigma(\bar{T}_3^4 - \bar{T}_4^4)}{1/\epsilon_3 + 1/\epsilon_4 - 1} \tag{47}$$

Radiation brings the midlayer temperature closer to the temperature of the outer wall having higher radiant intensity. As a result, unstable conditions are reached in one layer first and convection in the other layer is driven via the midlayer interaction. This behavior is similar to that found by Catton and Lienhard (1984) in parallel layers of unequal height, where the thicker layer drives convection in the thinner layer.

The general two-layer boundary conditions with semi-infinite outer walls are

$$D_1\Theta_1(-1/2) = \left\{\frac{a_1}{X_1} + N_1\Psi_a(\epsilon_1, \epsilon_2, a_1)\right\}\Theta_1(-1/2)$$

$$- N_2\Psi_b(\epsilon_1, \epsilon_2, a_1)\Theta_1(1/2) \tag{48}$$

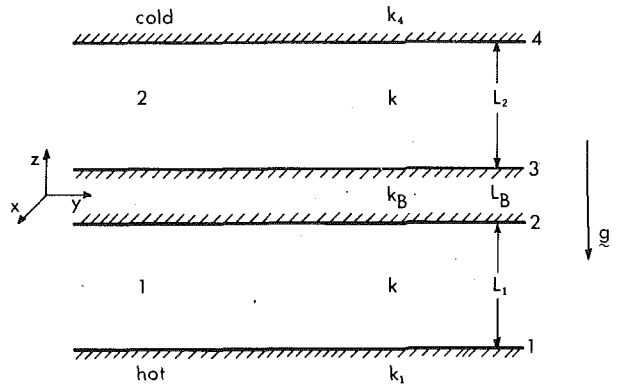

Fig. 6 Two-layer configuration

$$D_1\Theta_1(1/2)=\left\{\frac{a_1}{X_B}\left(\frac{\cosh(a_1A)-\alpha\sinh(a_1A)}{\alpha\cosh(a_1A)-\sinh(a_1A)}\right)\right.$$

$$\left.-N_2\Psi_a(\epsilon_2,\epsilon_1,a_1)\right\}\Theta_1(1/2)+N_1\Psi_b(\epsilon_2,\epsilon_1,a_1)\Theta_1(-1/2) \quad (49)$$

$$D_2\Theta_2(-1/2)=\left\{\frac{a_2}{X_B}\left(\frac{\cosh(a_2A)-\alpha\sinh(a_2A)}{\alpha\cosh(a_2A)-\sinh(a_2A)}\right)\right.$$

$$\left.-N_3\Psi_a(\epsilon_3,\epsilon_4,a_2)\right\}\Theta_2(-1/2)-N_4\Psi_b(\epsilon_3,\epsilon_4,a_2)\Theta_2(1/2) \quad (50)$$

$$D_2\Theta_2(1/2)=N_3\Psi_b(\epsilon_4,\epsilon_3,a_2)\Theta_2(-1/2)$$

$$-\left\{\frac{a_2}{X_4}+N_4\Psi_a(\epsilon_4,\epsilon_3,a_2)\right\}\Theta_2(1/2) \quad (51)$$

where $N_2=4\sigma L_1\bar{T}_3^3/k$, $N_3=4\sigma L_2\bar{T}_3^3/k$, $N_4=4\sigma L_2\bar{T}_4^3/k$, $A=L_b/2L_1$, and other terms are defined in the figure or have been defined previously. The groups N_2 and N_3 are fixed by N_1 and N_4 as part of the base state temperature profile. The parameter α represents the midlayer's conductive coupling between the two layers (Lienhard, 1987); it is iterated against a matching condition on the temperature gradients of the two layers

$$\mathrm{Ra}_1=\left(\frac{\bar{T}_1-\bar{T}_2}{\bar{T}_3-\bar{T}_4}\right)\left(\frac{L_1}{L_2}\right)^3\mathrm{Ra}_2 \quad (52)$$

For a solar collector type geometry, the simplest two-layer construction is a centered midlayer (under some circumstances, this is also the best configuration for convection suppression). The lowermost wall is liable to be highly conductive (typically copper, $X_1\approx 7\times 10^{-5}$) and blackened selectively. The uppermost wall will likely be glass, which has a large conductivity in comparison to air ($X_4\approx 0.03$) and is black in the infrared. The center layer is likely to be a thin plastic film of moderate conductivity ($X_B\approx 0.1$), preferably black in the infrared.

The high conductivity of the outer bounding surfaces, in conjunction with their relatively high thickness, allows them to be treated as isothermal; the thinness of the midlayer forces consideration of conductive effects there. The top wall and the midlayer may be modeled as black. The lowermost wall, when properly designed, will be gray and of low emissivity in the infrared ($\epsilon_1\approx 0.10$). For arbitrary ϵ_1, the boundary conditions are now

$$\Theta_1(-1/2)=0 \quad (53)$$

$$D_1\Theta_1(1/2)=\left\{\frac{a_1}{X_B}\left(\frac{\cosh(a_1A)-\alpha\sinh(a_1A)}{\alpha\cosh(a_1A)-\sinh(a_1A)}\right)\right.$$

$$\left.-N_2\Psi_a(1.0,\epsilon_1,a_1)\right\}\Theta_1(1/2) \quad (54)$$

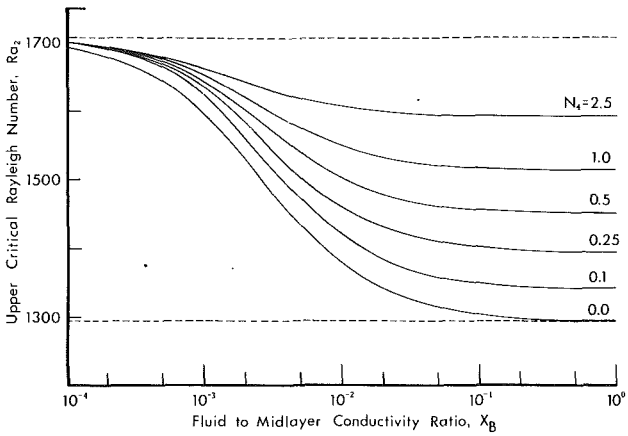

Fig. 7 Upper layer critical Rayleigh Number for $A=0.001$ and $N_1/N_4=2.0$ as a function of midlayer conductivity and radiation level

$$D_2\Theta_2(-1/2)=$$

$$\left\{\frac{a_2}{X_B}\left(\frac{\cosh(a_2A)+\alpha\sinh(a_2A)}{\alpha\cosh(a_2A)+\sinh(a_2A)}\right)+N_3\right\}\Theta_2(-1/2) \quad (55)$$

$$\Theta_2(1/2)=0 \quad (56)$$

where $a_1=a_2$. For simplicity, we focus on situations in which the bottom wall is simply black. A limited set of calculations outlines the effect of lower wall grayness.

Typical solutions are shown in Fig. 7 for a very thin midlayer ($A=0.001$). The behavior is very similar to that shown for a single layer in Fig. 3, but here radiation has a stabilizing influence at much smaller values of the conductivity ratio. The thin wall geometry has previously been found to be much more susceptible to finite conductivity effects since the boundary thinness allows greater temperature gradients to be supported; hence, radiation effects are much more pronounced at lower conductivities. For the two-layer case, in contrast to the single layer, radiation can be quite important for real materials.

Small effects of radiation on the base state temperatures result in the uneven spacing of the curves as $X_B\to 0$. Similarly, as $X_B\to\infty$, the critical Rayleigh number is slightly nonmonotonic, a small effect that we ignore for brevity. Both anomalies vanish as the radiation goes to zero.

Again, we offer a limited compilation of solutions in Table 2 while correlating a larger body of data in terms of the upper layer critical Rayleigh number

$$\Omega=\frac{1707.762-\mathrm{Ra}_c}{1707.762-\mathrm{Ra}_{\min}}$$

$$=\frac{1}{2}+\frac{1}{2}\tanh[a+b\ln X_B+c\ln(1+N_4)] \quad (57)$$

For $A=0.001$, exact values of the critical Rayleigh number spanning the ranges

$$0\le X_B\le 1.0,\quad 0\le N_4\le 2.5,\ \text{and}\ 1.0\le N_1/N_4\le 5.0 \quad (58)$$

yield the constants (a, b, c) as (2.9019, 0.50163, 0.24120) to an rms error *in the Rayleigh number* of 0.37 percent and a maximum error of 1.4 percent. Appropriate values of $\mathrm{Ra}_{\min}$ were extrapolated (to $\mathrm{Ra}_c\approx 3$) and fit as before

$$\Omega_{\min}=\frac{1707.762-\mathrm{Ra}_{\min}}{1707.762-1295.78}$$

$$=\frac{1}{2}+\frac{1}{2}\tanh[c+d\ln N_4+e\ln N_1] \quad (59)$$

A least-squares fit over the range

Table 2 Upper layer critical Rayleigh number and wavenumber for two layers with black walls and conducting midlayer: $N_1/N_4 = 2$, $A = 0.001$

Critical Rayleigh Number

	Fluid Layer to Wall Conductivity Ratio, X_B							
N_4	0	0.0003	0.001	0.003	0.01	0.03	0.1	1.0
0.0	1707.76	1668.56	1596.97	1483.85	1374.40	1325.09	1304.95	1296.71
0.1	1707.76	1683.58	1623.81	1518.53	1415.82	1369.72	1350.90	1343.23
0.25	1707.76	1686.21	1638.03	1548.95	1458.90	1418.19	1401.55	1394.30
0.50	1707.76	1687.32	1646.23	1574.99	1503.27	1470.66	1457.31	1451.83
1.00	1707.76	1688.20	1653.02	1599.76	1550.47	1528.63	1519.74	1516.01
2.50	1707.76	1689.64	1662.94	1631.77	1608.42	1599.08	1595.40	1593.64

Critical Wavenumber

	Fluid Layer to Wall Conductivity Ratio, X_B							
N_4	0	0.0003	0.001	0.003	0.01	0.03	0.1	1.0
0.0	3.116	3.038	2.898	2.708	2.590	2.562	2.554	2.552
0.1	3.116	3.060	2.921	2.737	2.630	2.605	2.599	2.597
0.25	3.116	3.070	2.957	2.788	2.690	2.667	2.662	2.660
0.50	3.116	3.074	2.985	2.852	2.772	2.752	2.747	2.746
1.00	3.116	3.077	3.008	2.923	2.873	2.86	2.858	2.857
2.50	3.116	3.082	3.039	3.004	2.990	2.987	2.987	2.987

Midlayer Coupling Parameter, α

	Fluid Layer to Wall Conductivity Ratio, X_B							
N_4	0	0.0003	0.001	0.003	0.01	0.03	0.1	1.0
0.0	∞	∞	∞	∞	∞	∞	∞	∞
0.1	∞	492.22	875.77	1177.9	772.12	335.42	111.00	11.525
0.25	∞	373.77	475.44	532.11	327.33	139.80	45.995	4.7642
0.50	∞	336.60	355.36	323.78	179.99	74.683	24.324	2.5183
1.00	∞	313.97	289.95	217.55	105.66	41.874	13.412	1.3756
2.50	∞	285.94	223.66	133.95	54.792	20.319	6.3437	0.64505

$$0 \le N_4 \le 2.5 \text{ and } 1.0 \le N_1/N_4 \le 5.0 \qquad (60)$$

gives (c, d, e) as (0.49225, 0.17771, −0.64288) to an rms error *in the Rayleigh number* of 0.78 percent and a maximum error of 1.5 percent. The values given by equation (59) intended for use with the preceding fit equation (57); they do *not* represent the limiting Rayleigh number as $X_B \to \infty$.

The above curve fits apply exactly only for $A = 0.001$. However, for small values of X_B, the parameter α becomes sufficiently large that the stability limit is characterized by the single parameter A/X_B, as was previously shown for thin midlayers in symmetric two-layer geometries (Lienhard, 1987). Hence, the critical Rayleigh number for thin midlayers of other A may be found as Ra_c for $A = 0.001$ from the correlation with X_B chosen so that A/X_B has the same value as the case of interest. For example, if we desire Ra_c for $A = 0.01$ and $X_B = 1.0$ (with $N_1 = 1.0$ and $N_4 = 0.5$), we may find it from the fit as Ra_c for $A = 0.001$ and $X_B = 0.1$ (at the same N_1 and N_4): The critical Rayleigh number for the unknown case is taken as 1457.31 from Table 2. The exact value calculated for the case of interest is 1457.11.

For $A \le 0.033$, this extrapolation procedure introduces errors of less than 1.1 percent over the entire range of X_B, N_1, and N_4 covered by equations (57) and (59). Errors decrease rapidly for thinner, more conductive midlayers and for lower levels of radiation. The extrapolation procedure provides a direct extension of the present results to other midlayer thicknesses.

Finally, we illustrate the effects of lower wall grayness for a plastic midlayer ($X_B = 0.1$) of aspect ratio $A = 0.01$, fairly common values for a solar collector partition. We vary only the radiation level and the lower wall emissivity, assuming the system to be otherwise the same as considered above (Table 3). As ϵ_1 decreases, the decreasing radiative exchange between the lower wall and the midlayer produces an increasing lower layer temperature difference. The Rayleigh numbers move in opposition, with Ra_1 decreasing and Ra_2 increasing. Consequently, control of the instability shifts from the upper layer at large ϵ_1 to the lower layer at small ϵ_1. As this change occurs, $1/\alpha$ passes from positive to negative values.[4]

[4]The parameter $\alpha = M/N$ (see equation (5)) characterizes the even/odd behavior of the temperature distribution. In all cases, onset of motion occurred for corotating cells (Lienhard and Catton, 1986) in the two layers with a predominantly even midlayer temperature distribution.

Table 3 Critical Rayleigh numbers for two layers with lowest wall gray: $N_1 = 1.0$, $N_4 = 0.5$, $A = 0.010$, and $X_B = 0.1$

ϵ_1	Ra_1	Ra_2	$\mathrm{Ra}_T \times 10^{-4}$	α	a
1.0	1300.74	1503.20	2.00	17.972	2.772
0.9	1348.27	1485.94	2.13	25.567	2.751
0.8	1393.44	1461.44	2.25	50.789	2.734
0.7	1433.49	1427.48	2.38	−53.669	2.726
0.6	1466.56	1382.84	2.49	−41.433	2.734
0.5	1491.54	1328.03	2.62	−22.032	2.754
0.4	1509.46	1265.14	2.74	−15.593	2.779
0.3	1522.06	1196.67	2.86	−12.549	2.802
0.2	1530.98	1124.74	2.98	−10.845	2.822
0.1	1537.45	1050.77	3.14	−9.7852	2.838

Table 4 Lower layer critical Rayleigh number and wavenumber for two layers with lowest wall gray: $\epsilon_1 = 0.1$, $A = 0.010$, and $X_B = 0.1$

Critical Rayleigh Number

	Upper Wall Radiation Number, N_4					
N_1/N_4	0.0	0.1	0.25	0.5	1.0	2.5
1.01	1374.38	1433.98	1486.78	1527.17	1560.62	1601.43
1.1	1374.38	1434.96	1488.08	1528.36	1561.71	1602.38
2.0	1374.38	1442.81	1498.06	1537.45	1570.13	1609.83
5.0	1374.38	1458.74	1516.34	1554.39	1586.45	1625.08

Critical Wavenumber

	Upper Wall Radiation Number, N_4					
N_1/N_4	0.0	0.1	0.25	0.5	1.0	2.5
1.01	2.590	2.631	2.714	2.812	2.897	2.983
1.1	2.590	2.633	2.717	2.815	2.899	2.985
2.0	2.590	2.646	2.741	2.838	2.918	3.000
5.0	2.590	2.673	2.787	2.880	2.952	3.022

The variation of the critical Rayleigh numbers with N_1 and N_4 for $\epsilon_1 = 0.1$ is shown in Table 4. The Rayleigh numbers are remarkably insensitive to N_1/N_4 over the range considered, but still respond strongly to N_4; the low levels of radiant exchange at the bottom wall are probably the cause of this behavior.

Table 3 also presents the *overall* Rayleigh number

$$\mathrm{Ra}_T = \left(\frac{g\beta}{\nu\alpha}\right)(L_1 + L_b + L_2)^3(\bar{T}_1 - \bar{T}_4) \qquad (61)$$

which characterizes the overall stability of a partitioned fluid layer. Overall stability *increases* as the lower wall emissivity decreases, a trend consonant with an intuitive view of the effects of lower wall grayness on the heat transfer, but in contradiction to the single-layer results. Although increasing radiant exchange raised the critical Rayleigh number of an individual fluid layer, the radiant equalization of the base state temperature differences increases overall stability as the lower wall emissivity drops. Evidently, the best two-layer solar collector design, in terms of convective or radiative top loss, is that with the lowest infrared emissivity at the absorber plate, in spite of the generally stabilizing effects of radiation found for a single fluid layer.

Two routes may be taken in determining a fluid layer's stability. The first is to regard N_1 and N_4 as being specified through a knowledge of T_1, T_4, and L_i, and then using the present data to determine whether or not convection occurs. The second route is to view only two of T_1, T_4, and L_i as being given, and to determine the value of the third parameter at which instability occurs. The latter case requires an iterative solution using the results for $\mathrm{Ra}(N_1, N_4)$: Each of Ra, N_1, and N_4 depend on two or more of T_1, T_4, and L_i.

5 Summary

The consequences of radiant heat exchange in Rayleigh–Bénard instability have been examined. Wall radiation through transparent gas layers has been incorporated into the usual boundary conditions for Bénard instability. Perturbations in the local net radiant heat transfer damp in-

stabilities, resulting in an increase in the critical Rayleigh number. The stabilization is independent of the specific planform at onset of motion, although the planform will still satisfy the Helmholtz equation.

In principle, thermal radiation may increase the critical Rayleigh number by as much as a factor of 2.5, but in practice the increase is smaller as a result of the low thermal conductivity of the gases considered. Solutions are given for a single fluid layer confined between identical, black, semi-infinite walls of finite conductivity and for a pair of fluid layers coupled by a conducting midlayer. For real materials, radiant effects are almost always negligible for a single layer confined by semi-infinite walls. For the two-layer case, however, radiant effects are substantial because the thinness of the midlayer accentuates the destabilizing effects of finite wall conductivity. The maximum overall stability for a two layer configuration is nevertheless achieved for a bottom wall of minimum infrared emissivity.

Acknowledgments

I am indebted to Professor D. K. Edwards and Professor I. Catton who originally called my attention to the possible importance of thermal radiation in Rayleigh–Bénard instability. This work was supported by the National Science Foundation under Grant No. CBT-8858288.

References

Bisshopp, F. E., 1960, "On Two-Dimensional Cell Patterns," *J. Math. Anal. Appl.*, Vol. 1, pp. 373–385.

Catton, I., and Lienhard V, J. H., 1984, "Thermal Stability of Two Fluid Layers Separated by a Solid Interlayer of Finite Thickness and Thermal Conductivity," ASME JOURNAL OF HEAT TRANSFER, Vol. 106, pp. 605–612.

Chandrasekhar, S., 1961, *Hydrodynamic and Hydromagnetic Stability*, Clarendon Press, Oxford, United Kingdom.

Edwards, D. K., and Sun, W. M., 1971, "Effect of Wall Radiation on Thermal Instability in a Vertical Cylinder," *Int. J. Heat Mass Transfer*, Vol. 14, pp. 15–18.

Hart, J. E., 1971, "Stability of the Flow in a Differentially Heated Inclined Box," *J. Fluid Mech.*, Vol. 47, pp. 547–576.

Lienhard V, J. H., 1987, "An Improved Approach to Conductive Boundary Conditions for Rayleigh-Bénard Instability," ASME JOURNAL OF HEAT TRANSFER, Vol. 109, pp. 378–387.

Lienhard V, J. H., and Catton, I., 1986, "Heat Transfer Across a Two Fluid Layer Region," ASME JOURNAL OF HEAT TRANSFER, Vol. 108, pp. 198–205.

Pellew, A., and Southwell, R. V., 1940, "On Maintained Convective Motion in a Fluid Heated From Below," *Proc. Roy. Soc. (London)*, Ser. A, Vol. 176, pp. 312–343.

Lord Rayleigh (John Wm. Strutt), 1916, "On Convection Currents in a Horizontal Layer of Fluid, When the Higher Temperature is on the Under Side," *Phil. Mag.*, Ser. 6, Vol. 32, No. 192, pp. 529–546.

Richards, R. F., and Edwards, D. K., 1989, "Effect of Boundary Radiation on Thermal Stability in Horizontal Fluid Layers," *Int. J. Heat Mass Transfer*, Vol. 32, pp. 81–86.

Siegel, R., and Howell, J. R., 1981, *Thermal Radiation Heat Transfer*, 2nd ed., Hemisphere, New York.

APPENDIX A

Generalized Third-Kind Boundary Conditions

Boundary conditions (33) and (34) applied to equation (1) produce the $\mathcal{C}_i$ indicated in the text as

$$\mathcal{C}_1 = -q_0 \sin(q_0/2) - (\Lambda_{21} + \Lambda_{22}) \cos(q_0/2) + 2\Re\left\{\frac{A}{A_0}[q \sinh(q/2) - (\Lambda_{21} + \Lambda_{22}) \cosh(q/2)]\right\} \tag{62}$$

$$\mathcal{C}_2 = q_0 \cos(q_0/2) + (\Lambda_{21} - \Lambda_{22}) \sin(q_0/2) + 2\Re\left\{\frac{B}{B_0}[q \cosh(q/2) + (\Lambda_{21} - \Lambda_{22}) \sinh(q/2)]\right\} \tag{63}$$

$$\mathcal{C}_3 = q_0 \sin(q_0/2) - (\Lambda_{11} + \Lambda_{12}) \cos(q_0/2) - 2\Re\left\{\frac{A}{A_0}[q \sinh(q/2) + (\Lambda_{11} + \Lambda_{12}) \cosh(q/2)]\right\} \tag{64}$$

$$\mathcal{C}_4 = q_0 \cos(q_0/2) + (\Lambda_{11} + \Lambda_{12}) \sin(q_0/2) + 2\Re\left\{\frac{B}{B_0}[q \cosh(q/2) + (\Lambda_{11} - \Lambda_{12}) \sinh(q/2)]\right\} \tag{65}$$

in which A/A_0 and B/B_0 may be evaluated from equations (4) and (5).